ISSN 2075-1133, Inorganic Materials: Applied Research, 2021, Vol. 12, No. 3, pp. 615–624. © Pleiades Publishing, Ltd., 2021.
Russian Text © The Author(s), 2020, published in Fizika i Khimiya Obrabotki Materialov, 2020, No. 5, pp. 11–23.

EFFECTS OF ENERGY FLUXES ON MATERIALS

Phase Transformations in Nitrided Ferrovanadium under the Action of a High Power Carbon Ion Beam

G. V. Potemkin[a], *, O. K. Lepakova[b], *, V. D. Kitler[b], M. V. Zhidkov[d], M. S. Syrtanov[a], **, and A. E. Ligachev[c], ****, *******

[a] *National Research Tomsk Polytechnic University, Tomsk, 634050 Russia*
[b] *Tomsk Scientific Center, Siberian Branch, Russian Academy of Sciences, Tomsk, 634055 Russia*
[c] *Prokhorov General Physics Institute, Russian Academy of Sciences, Moscow, 119991 Russia*
[d] *National Research Belgorod State University, Belgorod, 308015 Russia*
**e-mail: ep.gvp@yandex.ru*
***e-mail: maxim-syrtanov@mail.ru*
****e-mail: Klavdievna.K@yandex.ru*
*****e-mail: kemen7@mail.ru*
******e-mail: carbin@yandex.ru*

Received December 26, 2019revised July 20, 2020accepted August 17, 2020

Abstract—The phase and elemental composition of the near-surface layer of nitrided ferrovanadium irradiated with a high-power ion beam has been investigated by XRD and SEM methods. The impact of a powerful beam of the Temp-4M setup with an energy of carbon ions of 250 keV at a radiation pulse duration 10^{-7} s and a power density of charged particles $q_i \geq 10^6$ W/cm^2 causes melting of the Fe–VN composite and partial evaporation of elements with a high vapor pressure from the surface layer. High-speed solidification of the melt on the surface of the Fe–VN target leads to the formation of highly dispersed vanadium nitride and tetragonal carbide $Fe_{23}C_6$ in the modified layer. After irradiation of Fe–VN with a high-power beam with $q_i \approx 10^7$ W/cm^2 at a dose of ~ 10^{15} cm^{-2}, a violation of the translational invariance of the distribution of intercalated carbon atoms, a structural redistribution of Fe and V atoms, and the formation of X-ray amorphous microliquations of Fe–V and gas–carbon complexes are observed in the modified layer.

Keywords: Fe–VN, high power ion beam, structural-phase state

DOI: 10.1134/S207511332103031X

INTRODUCTION

The action of powerful beams of charged particles on a condensed medium with specified properties is determined by the particle energy E_i, the power density q on the target surface, and the radiation pulse duration τ [1–4]. The energy range of charged particles of powerful beams used to modify the properties of the surface layer is in the range from several tens of keV to several hundred keV [1, 5–11]. When a substance is irradiated with a powerful ion beam (PIB), in contrast to the action of powerful electron beam (PEB), the initial medium turns into a solution or a multiphase material, where the introduced impurities are both the components of the beam and the atoms of the atmosphere of the working chamber. The substances formed during the interaction of the PIB with the material always depend on the type of ions of the powerful beam.

The study of structural-phase transformations in processed materials under the influence of PIB (without taking into account shock-wave effects) is a very important task for clarifying the details of the processes occurring in the surface layer of a substance when it is doped with the fluence of carbon ions n_i with power density of $q_i = 10^5$–10^8 W/cm^2 and kinetic energy of particles up to 1 MeV, causing heating, melting, and evaporation of the irradiated material. From the viewpoint of technology, for processing PIB products, it is important to know both the melting point T_m of the irradiated surface layer of the material and the value of the corresponding ion fluence n_i and the power density of the beam on the target surface q_c.

The study of the effect of PIB on composite materials makes it possible to evaluate the efficiency of simultaneous irradiation of different components of the material and their interaction with each other. Previously, such studies were carried out only on homogeneous metals and alloys [8, 10–16].

MATERIALS AND METHODS

Samples for research were cut from a composite material Fe–VN obtained using the SHS process with

Table 1. Elemental composition of the original sample

Mass fraction, %									
base			impurity content						
Fe	V	N	C	Si	Mn	Al	As	P	S
44.4	47.08	9.8	0.18	1.0	1.6	0.2	0.01	0.07	0.02

VN grains 3–5 μm in size located in the α-Fe matrix [17]. The elemental composition of the sample is shown in Table 1.

The experiments were carried out on a Temp-4M accelerator operating in a two-pulse mode [18–20]. The samples were irradiated in a vacuum diode with a focusing geometry of the ion flow with a dose of D = 30 pulses at an energy of singly charged ions E_i = 250 keV. The experiments were carried out at two different ion fluences (Fig. 1): mode I—the maximum ion fluence in the pulse is $n_{max} \sim 10^{14}$ cm^{-2}, the target in focus (position *6*), and mode II—the average ion fluence in the pulse is $n_i \approx 10^{13}$ cm^{-2}, target out of focus (position *5*). The duration of the radiation pulse at half maximum was τ = 100 ns at a pulse repetition rate of 1 Hz. The flow of charged particles extracted from the complex plasma using a multi-aperture anode consisted of atomic (mainly C_{12}^+) and molecular cluster particles of carbon C_n^+ and neutrals C_n in the form of stable carbon clusters with different numbers of atoms [21, 22]. According to the estimates of [19], the fraction of protons in PIB did not exceed ~10%. For simplicity, further we will assume that the PIB consists only of C_{12}^+ ions. Ion flux power density q_i for a TEMP-4M installation is in the range of $q_i \approx E_i n_i/\tau \approx 4 \times 10^6$–$10^8$ W/cm$^2 \gg q_c$ of the critical heat flux, which determines the threshold of destruction of metals in the framework of the phenomenological model under the action of the PEB [1, 2].

The phase composition and structure of the surface layers of the irradiated samples were investigated using a Shimadzu XRD 7000S diffractometer in Cu K_α radiation in Bragg-Brentano geometry at 40 kV and 30 mA. Diffraction measurements were carried out in the grazing incidence geometry at an angle of 3°.

The surface morphology and composition of the modified layer of the sample were studied using a Philips SEM 515 scanning electron microscope with an EDAX energy dispersive attachment, as well as an FEI Quanta 600 microscope with an EDAX spectrometer (with an EDX resolution of 0.2% on Be).

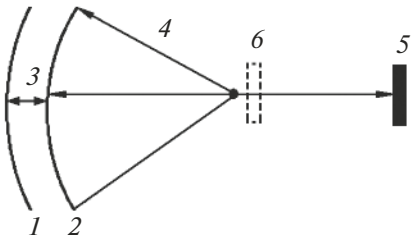

Fig. 1. Diagram of the setup for irradiation of specimens with power ion beam: (*1*) potential electrode; (*2*) grounded electrode; (*3*) interelectrode distance; (*4*) focal length; (*5*) target position out of the focus (mode II); (*6*) target position in the focus (mode I).

RESULTS AND DISCUSSION

An idea of the spatiotemporal evolution of the state of the material can be obtained by considering the process of action of a single pulse of a powerful ion beam on the surface of an irradiated target.

As is known, the impact of PIB on condensed media is a set of nonlinear processes associated with both high-speed heating of the target [1–4] and with the introduction of impurities into the surface layer in the form of particles that make up the beam and, possibly, atoms of the atmosphere of the working chamber. The specific energy stored in the bulk of an irradiated material per one pulse is much higher than in the case of irradiation with electrons at the same parameters (energy, current, pulse duration) of the particle beam. The threshold energy of the formation of lattice defects for light ions is $E_d < 10^2$ eV, while for electrons it is in the range from 10^4 to 10^6 eV [5, 23, 24].

The interaction of ions with a condensed medium can be geometrically described using the parameters characterizing the range of ions: the effective range $R^* = R_p + \Delta R_p$, the mean projective (longitudinal) range R_p, the root-mean-square deviation in the longitudinal direction ΔR_p, and the root-mean-square deviation of the ions in the transverse direction (transverse range) ΔY [5, 9, 24, 25]. A layer of substance with a thickness equal to the depth of the effective range R^* of the C_{12}^+ ion of given energy, we will call the running layer. Table 2 shows geometric characteristics of the interaction of C_{12}^+ ions with energy of 250 keV with a Fe–VN target.

Accelerated ions create cascades of atomic collisions in the target material with the density of the released energy in a single cascade in the range of 10^{-3}–10 eV/atom, and the number of atomic collisions on the path length of one ion reaches $N_c \approx 10^6$–10^7 [5, 9, 23, 24]. A cascade of collisions forms a typical spatial

region with an outer shell of interstitial atoms and an inner core enriched in vacancies. Frenkel pairs (vacancies and interstitial atoms) diffuse along the lattice until absorption at the boundaries between phases and grains and at other imperfections of the structure. Irradiation of the target with powerful beam of light ions (from carbon and higher) with energy of hundreds of keV leads to the spatiotemporal overlap of dense collision cascades, while some of the atoms are displaced from the lattice sites (N generations of displaced atoms), and the others transition into an excited state with large vibration amplitudes relative to the equilibrium position [3, 23, 24]. In this case, the crystal lattice of the material turns out to be completely or partially destroyed. The mixing of the cascades leads to the formation of a zone in the surface layer of the target, in which free energy of atoms and entropy are much higher than in the rest of the heated target [5, 26, 27].

In a phenomenological description of the processes occurring during a PIB pulse, the rate of phase transformations in the surface layer depends on the fraction of energy consumed on local heating of the layer, the thickness R^* of which is equal to the effective range of a carbon ion of a given energy in the material, and on the transfer of heat due to thermal conductivity from the running layer to the target volume.

High particle flux density on the target surface and short pulse duration create favorable conditions for disordering and amorphization of the material under the action of PIB. Under these conditions, "dynamic" melting (when the Lindemann condition is satisfied) precedes thermal melting [28]. During PIB irradiation of a condensed medium, thermal conductivity in the layer of the target material significantly decreases owing to the scattering of phonons and conduction electrons on surface and bulk defects generated by the ion beam and a corresponding decrease in their mean free path [29].

The distribution of energy losses over depth for C_{12}^+ carbon ions and protons is characterized by the presence of a rather extended region of slow dose growth with increasing depth and ends with a sharp Bragg peak [25, 30], whose amplitude in the energy range up to 1 MeV by a factor of 6–13 exceeds the energy loss of ions on the surface.

The volume of interaction of a homogeneous monochromatic ion beam with a target is limited by the beam size on the target and the effective path of ions R^*. Within the framework of the phenomenological description of the interaction of a particle beam with a target, the depth of the material layer heated up during the pulse duration τ is $L = (\alpha\tau)^{1/2}$, where $a = \lambda/\rho c$ is the thermal diffusivity, λ is the thermal conductivity, ρ is the density, and c is the heat capacity of unirradiated material [1, 2]. When a target is exposed to PIB, the values of λ, ρ, and c depend not only on temperature [1, 2, 4] but also on the chemical composition of the running layer, which changes during irradiation with ions, which is fundamentally different from the case of irradiation with an electron beam. The use of thermal parameters of an undisturbed medium to estimate the thickness of the heated layer, as under the action of a powerful electron beam (PEB) or laser radiation (LR), for PIB gives, at best, upper limit of this value and leads to significant overestimation of the thickness of this layer. However, at depths significantly exceeding the thickness of the modified layer $R^* + L$, the use of thermal parameters of an undisturbed medium is quite acceptable for thermal calculations.

Table 2. Geometric parameters of interaction of C_{12}^+ ions with substance

Parameter/element	R_p, μm	ΔR_p, μm	ΔY, μm	L^*, μm
Fe	0.243	0.065	0.076	1.5
VN	0.286	0.077	0.089	–

* Depth of the layer heated up during the action of one pulse.

During the radiation pulse, the total number of displaced and excited target atoms N^* in the zone of effective ion path can be determined as $N^* = n_i N_c$, which is much larger than the number of atoms in the path $N_0 = SR_p n_a$, where n_a is the atomic concentration of the substance and S is the surface area. At normal incidence of PIB on the surface, a disk-shaped heat source with a thickness of ~$2\Delta R_p$, enhanced by the Bragg effect, is created inside the target at a depth of ~R_p.

For ions with energies up to 1 MeV, the thickness of the melt formed on the target surface under the action of PIP is determined by the beam power density q_i and the duration of the radiation pulse τ. At a pulse repetition rate of 1 Hz, the surface layer of the target does not have time to cool down to the initial temperature before the arrival of the next pulse; in this case, each subsequent pulse increases the lifetime of the melt and the depth of the heat-affected zone until dynamic equilibrium is established between the heat input from the beam and heat losses in the running layer.

The energy required for evaporation of the substance can be estimated as $E_v = V[\rho c(T_m - T_0) + \Delta H_m + \rho c(T_v - T_m) + \Delta H_B]$, where $T_0 = 20°C$ is the initial temperature of the sample in the chamber; V is the volume of the heated material; T_m and ΔH_m are the temperature and the specific heat of fusion; and T_v and ΔH_B are the temperature and the specific heat of vaporization, respectively [1, 2]. The thermal parameters of the elements and compounds that make up the nitrided ferrovanadium, as well as the elemental composition of the Fe–VN surface, are given in Table 3.

A rapid increase in the power density of the ion beam, corresponding to the leading edge of the PIB radiation pulse [18–20], leads to redistribution of the

Table 3. Thermal characteristics of elements and compounds composing the target material

Element	ρ, kg/m^3	T_m, °C	ΔH_m, kJ/kg	ΔH_v, MJ/kg	P_v **, Pa	a, m^2/s	T_v *** , °C
Fe	7870	1538	277	6.3	10^{-1}	20.9	1170
V	6120	1917	452	9.5	10^{-1}	10.2	1540
C	2266*	subl. 3652	27900	59	10^4 *	3.6	1890
Mn	7470	1244	266	4.2	1	2.14	780
Si	2330	1415	177	12.6	10^{-1}		1090
VN	6102	2050*	376	*	1.3*	5.9	*

* Decomposition temperature of VN is close to T_m also in vapor over vanadium nitride V/N ~ 0.06–0.04; that is, nitrogen also evaporates, and vanadium remains in the melt [31, 32].
** Saturated vapor pressure P_v (Pa) at melting point T_m.
*** Temperature T_v (°C) at which vapor pressure P_v of the substance becomes equal to the initial pressure in the working chamber of ~10^{-2} Pa.

beam energy in the material, which is scattered due to thermal conductivity $Q_t = V[\rho c(T_m - T_0) + \Delta H_m + \rho c(T_v - T_m)]$ and consumed for defect formation and evaporation of the irradiated material $Q_s = V\Delta H_B$. The transition of the near-surface layer of the irradiated material from the stage of defect formation and heating to evaporation leads to the formation of two movable interfaces: solid–liquid and liquid–vapor.

Table 4 shows the data of X-ray microanalysis of the surface of nitrided ferrovanadium before irradiation. As one can see, within the sensitivity of the method at the electron probe energy of 30 keV, grains of vanadium nitride are clearly observed in the surface layer of the iron matrix with no carbon and oxygen in the matrix. Almost all impurities of the nitrided ferrovanadium obtained by the SHS method are concentrated in the α-Fe matrix [17, 31].

The process of phase transitions with melting and evaporation fronts that move inside the target according to the direction of the heat flow until the melting front stops completely is usually considered as a nonlinear nonstationary Stefan problem with two moving boundaries. For an open dissipative system (melt) exchanging energy and matter with the external medium (powerful beam of ions), stopping of the melting front is a bifurcation point. At this point, the dissipative system (melt) in the process of rapid solidification loses the properties of uniqueness and stability. At the same time, microstructures both related to the initial one and fundamentally different from it start to grow [27, 33, 34].

Table 4. Elemental composition of the initial sample of Fe–VN composite material

Element	VN grains, at %	Fe bunch, at %
Fe	7.1	42.6
V	59.5	29.8
N	30.2	18.4
Si	1.7	4.4
Mn	1.5	4.9

Doping of the melt to a depth greater than R^* due to diffusion of C_{12}^+ ions is determined by the lifetime of the liquid film on the surface of the irradiated material and the rate of its cooling on a solid crystallizer (target thickness is $d \gg R^* + L$) [35, 36].

At athermal implantation, when $q_i \times 10$–10^2 W/cm^2 [7, 9, 25], a profile of the distribution of implanted atoms with a maximum near R^* is formed in condensed media, which is quite different in the case of fluence of ions bombarding the target $n_i \times 10^{13}$ cm^{-2} [25, 32]. For a homogeneous monochromatic ion beam and a homogeneous target, in this case, translational invariance of the profile of implanted impurity atoms is always observed in the entire volume of the running layer [7, 9, 25].

The results of the impact of PIB on the irradiated material substantially depend on the power density q_i and dose D at constant energy of carbon ions. In the peripheral zone of exposure of the beam, where $q_i < 10^6$ W/cm^2 and $n_i < 10^{13}$ cm^{-2} (mode II), where the edge inhomogeneity of the beam power density is noticeable, selective evaporation of the α-Fe matrix is observed at insignificant melting of the VN grain surface (Fig. 2).

In this case, differences in the thermal properties of the components that make up the nitrided ferrovanadium are manifested, and the specific energy of the beam released in the irradiated layer is higher than the specific heat of vaporization of iron ΔH_v, but insufficient for vaporization of vanadium nitride (Table 3). The low-melting α-Fe matrix with impurities evaporates, and refractory VN grains form a "scattered cobblestone" relief (Fig. 2). Figure 2 also shows protruding grains of slightly melted VN, similar in size to the original unirradiated grains. The cavities between the grains indicate a fairly large amount of evaporated iron, which is quite consistent with the difference in thermal parameters of VN and α-Fe.

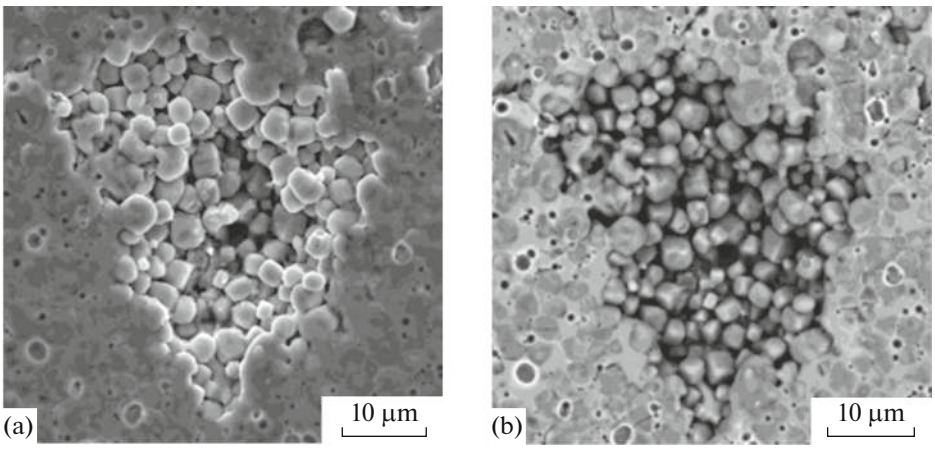

Fig. 2. Surface of the composite irradiated with ions in mode II. Images: (a) in secondary electrons; (b) in reflected electrons.

Cracks are clearly visible on the solidified surface of many VN grains after irradiation in this mode (Fig. 3). Obviously, strong internal stresses arise in the vanadium nitride grains partially melted from the top, leading to the appearance of cracks, which is typical of materials with a wide temperature range of solidification [34].

When the surface of nitrided ferrovanadium is irradiated with a beam of carbon ions with a fluence of $n_i < 10^{13}$ cm^{-2} and $q_i < 10^6$ W/cm^2 (mode II), in the peripheral zone of the beam, where its edge inhomogeneity is manifested, linear traces of selective evaporation are observed in the form of sequentially connected α-Fe depressions, craters, and cracks on the melted surface of VN grains (Fig. 4). In this case, a branched network is formed on the solidified surface of the irradiated material in the form of chains consisting of depressions in the region of existence of α-Fe and craters and cracks on VN grains.

At maximum fluence n_{max} and $q_{max} > 10^6$ W/cm^2 (mode I), when the thickness of the molten layer of the composite material is comparable to the grain size of VN, cracking of grains after solidification is weak, since VN grains are covered with a multicomponent quasi-amorphous alloy (Figs. 5–8). After irradiation in mode I, a continuous liquid film is formed on the sample surface, since the target material melts to the depth of the thermal influence $L_0 = R^* + L$, which is different for α-Fe and VN grains. In this case, specific energy ε released by the beam in the irradiated layer of the substance exceeds the latent heat of evaporation ΔH_v of both α-Fe and vanadium nitride (Table 3). At the maximum power density of the ion beam q_{max} in mode I, differences in thermal properties of VN and α-Fe in the irradiated material are leveled, and a continuous liquid film of a complex chemical composition is formed on the surface (Fig. 5). All impurity elements with high values of vapor pressure (Mn, Si, Al, etc.) are removed from the irradiated layer (Table 4).

In addition to atomic and molecular carbon ions, the Temp-4M installation contains a significant amount of neutral particles consisting of some carbon atoms and isolated hydrogen atoms. All these carbon particles and hydrogen atoms can form volatile compounds with metal atoms in a liquid or vapor state (for example, VC, VC_2, VC_4, etc.), which naturally reduces the concentration of carbon atoms in the modified layer. However, all this does not significantly affect the nature of the spatial distribution of carbon in this layer.

At the initial stage of irradiation, before the target surface layer melts, the spatial redistribution of Fe, V, and N atoms and intercalated carbon and oxygen atoms occurs owing to cascade processes and radiation-induced segregation that is controlled by the fluxes of Frenkel defects [23, 24, 26]. Further action of PIB on the surface of the sample leads to melting of the running layer and implementation of hydrodynamic mechanisms of heat and mass transfer in it. Temperature and carbon concentration gradients aris-

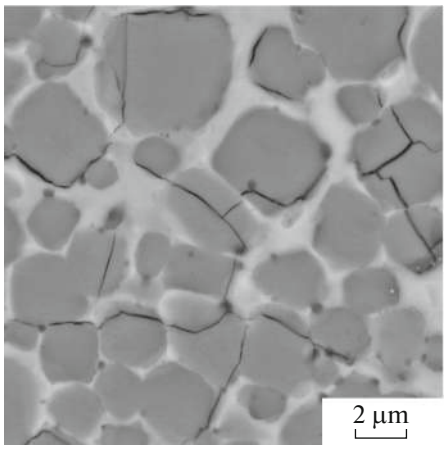

Fig. 3. SEM images in reflected electrons of the cracks on the solidified Fe–VN surface.

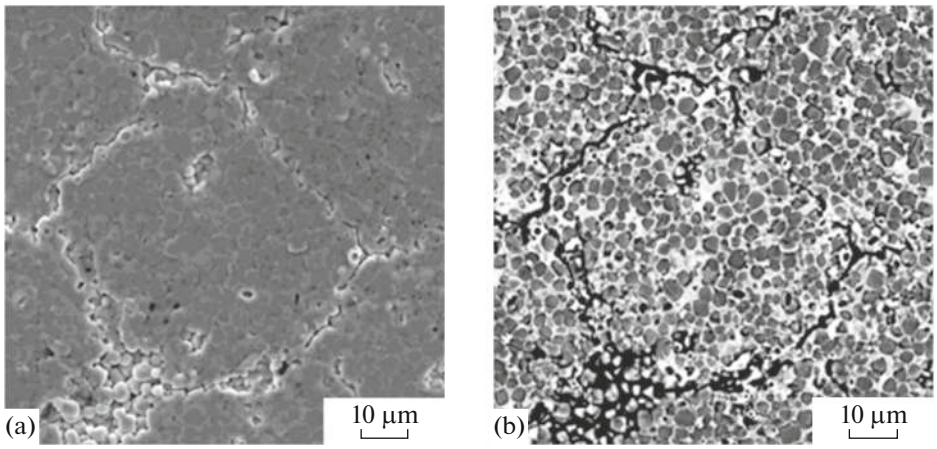

Fig. 4. SEM images in secondary (a) and reflected (b) electrons of the target surfaces irradiated in mode II.

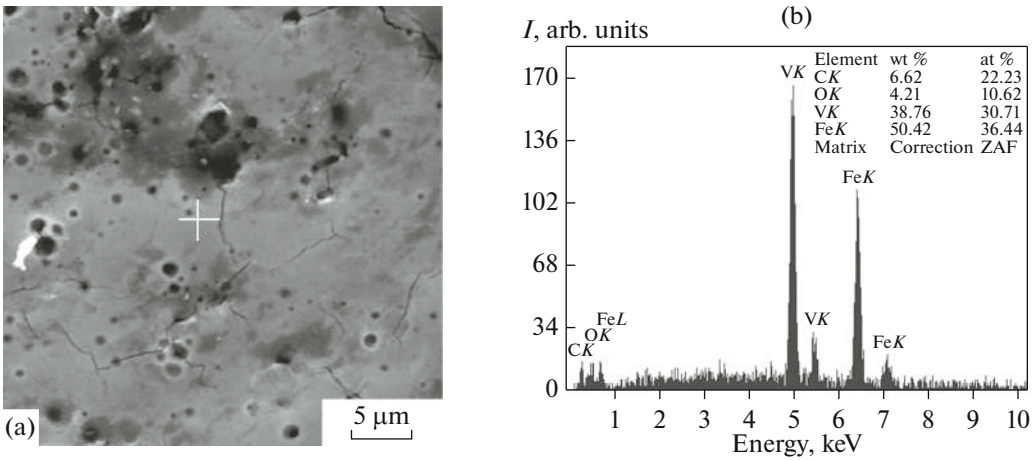

Fig. 5. SEM image of Fe–VN surface irradiated in mode I (a) and elemental composition near the surface layer of solidified melt (b).

ing between the internal heat source located at the depth R^* and the free surface of the liquid lead to the initiation of a complex process of heat and mass transfer. The final stage of structural-phase transformations occurring under the action of PIB is high-speed quenching of the melt of the surface layer of the irradiated sample from the Fe–VN composite [27, 28, 33, 34].

The mechanisms of heat and mass transfer in the liquid layer during the beam action have not been determined [27, 32, 35, 36]. After passing the time point of bifurcation in the volume of the solidifying melt under conditions of locally nonequilibrium solidification, a structure with a locally nonequilibrium chemical composition is formed. Depending on the propagation rate of the heat front, a transition to the mechanism of diffusionless, that is, chemically nonselective, solidification is possible. Figures 5–7 show data on the appearance of X-ray amorphous complexes of the metal–gas type ($Me_1Me_2G_1G_2$) (Figs. 5, 7), gas–carbon (Figs. 6c, 6d) and Fe–V (Figs. 6a, 6b) compounds in the solidified layer.

The distribution of chemical elements in the material after irradiation at q_{max} (Figs. 5–8) differs significantly from the initial one (Fig. 3), while clear boundaries between the VN grains and the α-Fe bond are not observed (Figs. 5, 6).

Owing to high-speed solidification at the liquid–solid interface, solid phase nuclei appear both by the diffusion-free crystallization mechanism and as a result of diffusion-controlled crystallization of highly dispersed VN grains (Table 5) [27]. The speed of advancement of the solidification front in the alloy on the target surface has a significant effect on the formation of various quasicrystalline microstructures. Nonequilibrium conditions arising at the interface also lead to the appearance of metastable phases such as $Fe_{23}C_6$ carbide with a face-centered tetragonal lattice in the cooling melt. The high cooling rate of the melt ($\sim 10^9$ s^{-1}) promotes the formation of highly dispersed

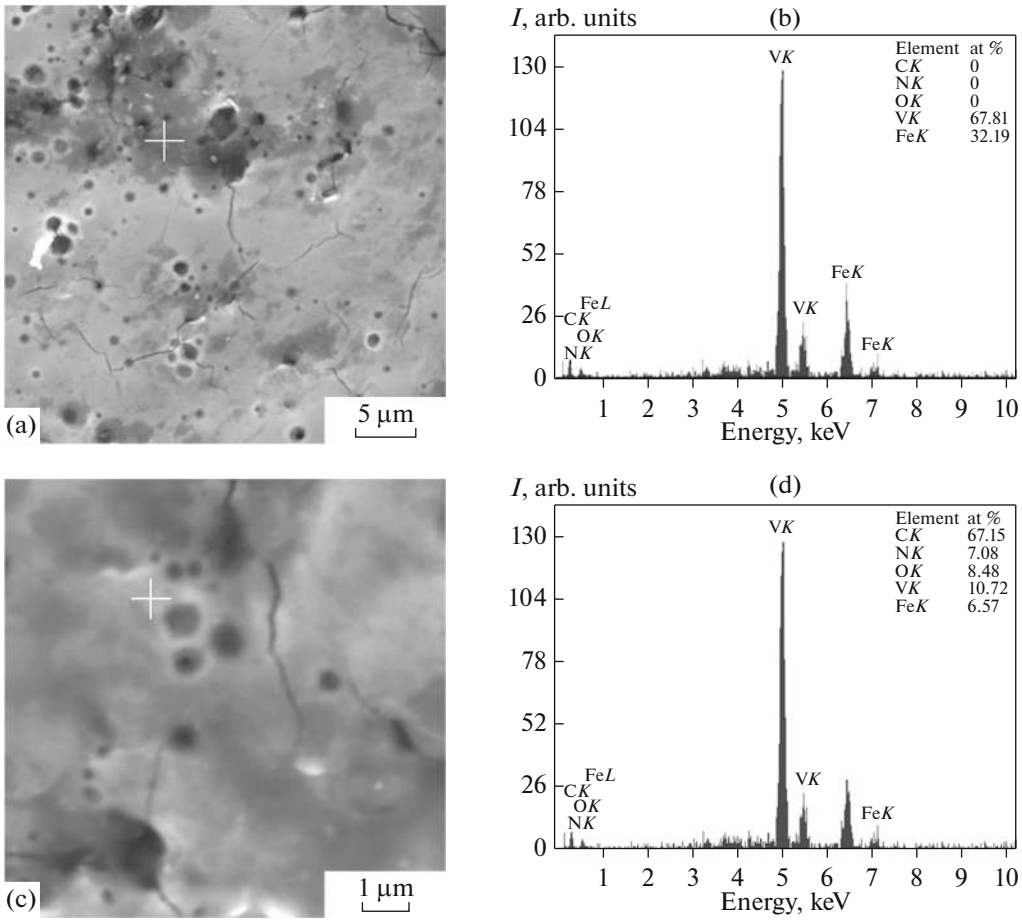

Fig. 6. Segregation of elements in the surface layer of a solidified melt of nitrided ferrovanadium irradiated in mode I: (a, c) SEM images of the surface, points of analysis of the elemental composition are marked with a cross; (b, d) EDAX spectra and the content of elements at the analyzed points.

VN in the solidified layer of the material. Figure 8 shows diffraction patterns of the irradiated layer of nitrided ferrovanadium before and after treatment of the material with a beam in mode I.

The distribution of chemical elements in the modified layer of material after PIB irradiation is influenced by the gaseous atmosphere of the working chamber, the composition of which changes significantly during the formation of carbon plasma [37, 38]. During the action of the plasma pulse, a pressure jump occurs in the chamber of the Temp-4M installation, since from the surface of a potential electrode made of reactor graphite, along with carbon vapor (C_1, C_2, C_3, C_4, C_5), hydrogen, oxygen, carbon monoxide, CH,

Table 5. Results of X-ray investigation of the samples irradiated in mode I

Sample	Phases	Content of phases, vol %	Lattice parameters, Å	Size of crystallites, nm	Microstresses, $(\Delta d/d) \times 10^{-3}$
Fe–VN	α-Fe (BCC)	28.9	$a = 2.870$	22	1.1
	VN (FCC)	71.1	$a = 4.110$	26	1.5
Fe–VN + C	α-Fe (BCC)	25.4	$a = 2.863$	21	1.9
	VN (FCC)	70.0	$a = 4.119$	13	2.7
	$Fe_{1.92}C_{0.48}$ (FCT)	4.6	$a = 2.856$	39	0.9
			$c = 2.954$		

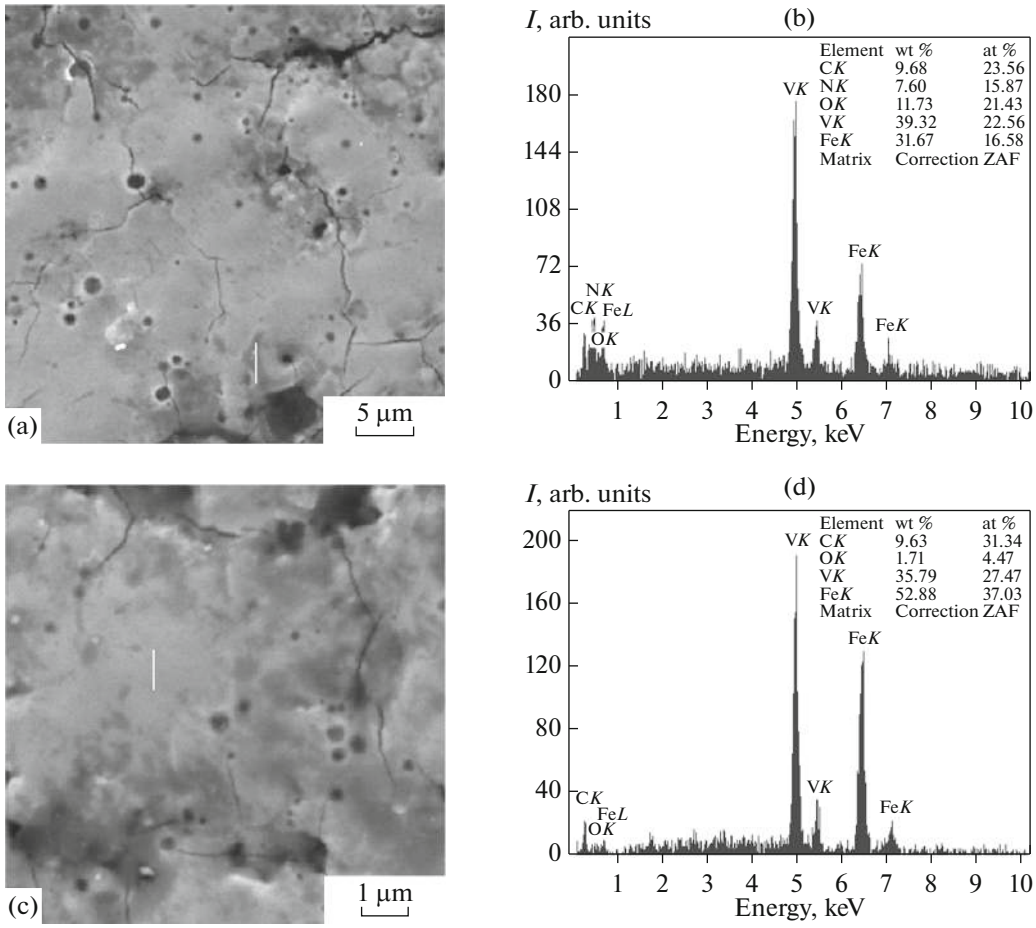

Fig. 7. SEM image of the solidified surface of nitrogenous ferrovanadium irradiated with PIB in regime I (a, c) and the effect of power ion beam irradiation on the elemental composition of the modified layer (b, d).

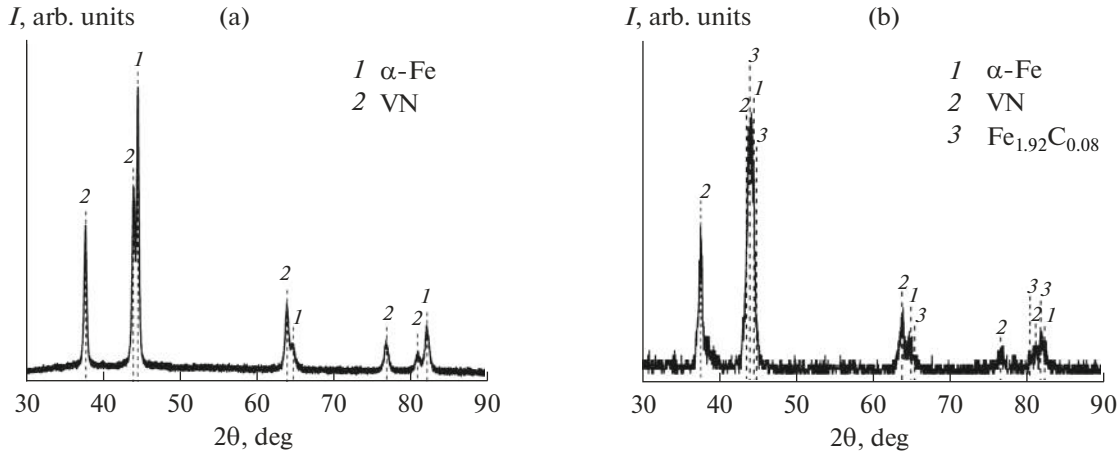

Fig. 8. Diffraction patterns of the ferrovanadium before (a) and after ion irradiation in mode I (b).

CN, etc., are released, the solubility of which is high in the melt [32, 35, 36]. The oxygen concentration in the solidified melt reaches tens of percent (Fig. 7), which indicates a significant role of the process of saturation of the melt with oxygen atoms, traces of which are absent in the initial Fe–VN.

CONCLUSIONS

1. It has been shown that, to assess the effects of PIB with energy of charged particles up to 1 MeV on composite materials, it is impossible to use the phenomenological approach without taking into account the discrete structure of the substance and a nonlinear

nature of the interaction of a beam of bombarding particles with a condensed medium.

2. It is also impossible to establish the melting point of composite materials during PIB irradiation, since before melting the irradiated layer of the substance passes into an amorphous state.

3. Under the influence of PIB with high power density of $q_{max} > 10^6$ W/cm^2, the target material transforms into a substance with a different composition and structure, and at doses of more than 10^{14} ions/cm^2, in the surface layer is formed a material with a broken translational invariance of the distribution of carbon atoms and microliquations from the atoms of chemical elements of the irradiated material, beam ions, and atoms of the atmosphere of the working chamber.

4. The formation of microliquations in the form of X-ray amorphous complexes of ferrovanadium and complexes consisting of carbon atoms (50–70 at %), metal, and gases can be explained by the influence of convective mixing and radiation-induced segregation.

5. During cooling of the melt of the irradiated PIB material, the mechanisms of zero-diffusion and crystalline solidification are implemented.

ACKNOWLEDGMENTS

We are grateful to A.I. Pushkarev and S.V. Pavlova for help in irradiating the samples and to G.E. Remnev for useful discussions.

REFERENCES

1. Rykalin, N.N., Uglov, A.A., and Zuev, I.V., *Osnovy electronnoluchevoi obrabotki materialov* (Principles of the Electron-Beam Treatment of Materials), Moscow: Mashinostroenie, 1978.
2. Veiko, V.P., Libenson, M.N., Chervyakov, G.G., and Yakovlev, E.B., *Vzaimodeistvie lazernogo izlucheniya s veshchestvom* (Interaction of Laser Radiation with Matter), Moscow: Fizmatlit, 2008.
3. Artemov, V.A., Vlasov, M.A., Malafeev, O.A., Reder, A.V., Rykhlov, A.V., and Safonov, V.A., Experimental study of nonstationary evaporation of metal under the action of an electron beam, *Zh. Tekh. Fiz.,* 1978, vol. 48, no. 1, pp. 192–193.
4. Zalyubovsky, I.I., Kalinichenko, A.I., and Lazurik, V.T., *Vvedenie v radiatsionnuyu akustiku* (Introduction to Radiation Acoustic), Kharkov: Vishcha Shkola, 1986.
5. Thompson, M.W., *Defects and Radiation Damage in Metals*, Cambridge: Cambridge Univ. Press, 1969.
6. Potemkin, G.V. and Lepakova, O.K., Modification of the surface properties of high-dispersion AlB_{12} by a power beam of carbon ions, *Fiz. Khim. Obrab. Mater.*, 2014, no. 6, pp. 5–12.
7. *Ion Implantation*, Hirvonen, J.K., Ed., New York: American, 1980.
8. Pogrebnyak, A.D., Remnev, G.E., Chistyakov, S.A., and Ligachev, A.E., Modification of the properties of metals by high-power ion beams, *Sov. Phys. J.*, 1987, vol. 30, no. 1, pp. 39–48.
9. Komarov, F.F., *Ionnaya implantatsiya v metally* (Ion Implantation in Metals), Moscow: Metallurgiya, 1990.
10. Korotaev, A.D., Tyumentsev, A.N., Pochivalov, Yu.I., Ovchinnikov, S.V., Remnev, G.E., and Isakov, I.F., Phase composition and defect structure in the surface layer of metal targets irradiated by high power ion beams, *Phys. Met. Metallogr.*, 1996, vol. 81, no. 5, pp. 542–548.
11. Kovivchak, V.S., Panova, T.K., and Mikhailov, K.A., Surface structuring of polycrystalline magnesium under the action of high-power ion beam of nanosecond duration, *Tech. Phys. Lett.*, 2010, vol. 36, no. 12, pp. 1092–1094.
12. Volkov, N.B., Maier, A.E., and Yalovets, A.P., On the mechanism of cratering on solid surfaces exposed to an intense charged particle beam, *Tech. Phys.*, 2002, vol. 47, no. 8, pp. 968–977.
13. Potemkin, G.V., Ligachev, A.E., Zhidkov, M.V., Kolobov, Yu.R., Remnev, G.E., Gazizova, M.Yu., Bozhko, S.A., and Bureev, O.A., The change in the surface topography of magnesium under high-flux C^+ ion irradiation, *Fiz. Khim. Obrab. Mater.*, 2015, no. 4, pp. 5–9.
14. Remnev, G.E. and Shulov, V.A., Application of high-power ion beams for technology, *Laser Part. Beams,* 1993, vol. 11, no. 4, pp. 707–731.
15. Zhidkov, M.B., Ligachev, A.E., Potemkin, G.V., Manokhin, S.S., Remnev, G.E., and Kolobov, Yu.R., Study of the structure of crater at the surface of 12Cr18Ni10Ti steel irradiated by high-power pulsed ion beam, *Inorg. Mater.: Appl. Res.,* 2018, vol. 9, no. 3, pp. 376–378.
16. Potemkin, G.V., Ligachev, A.E., Zhidkov, M.V., Kolobov, Yu.R., Remnev, G.E., Smolyakova, M.Yu., and Bozhko, S.A., The change in the surface topography of magnesium under high-flux C ion irradiation, *Izv. Vyssh. Uchebn. Zaved., Fiz.*, 2014, vol. 57, no. 10-3, pp. 221–225. https://www.elibrary.ru/item.asp?id=22980234.
17. Maksimov, Yu.M., Chukhlomina, L.M., Braverman, B.Sh., and Smirnov, L.A., *Samorasprostranyayushchiisya vysokotemperaturnyi sintez azotsoderzhashchikh splavov dlya metallurgii* (Self-Propagating High-Temperature Synthesis of Nitrogen-Containing Alloys for Metallurgy), Novosibirsk: Nauka, 2014.
18. Logachev, E.I., Remnev, G.E., and Usov, Yu.P., Acceleration of ions from an explosive-emission plasma, *Pis'ma Zh. Tekh. Fiz.*, 1980, vol. 6, no. 22, pp. 1404–1406.
19. Isakov, I.F., Kolodii, V.N., Opekunov, M.S., Matvienko, V.M., Pechenkin, S.A., Remnev, G.E., and Usov, Yu.P., Sources of high power ion beams for technological applications, *Vacuum*, 1991, vol. 42, no. 1/2, pp. 159–162.
20. Pavlov, S., Ligachev, A., Potemkin, G., and Remnev, G., Mass transfer between electrodes of a magnetically insulated diode operated in two pulse mode, *Proc. 11th Int. Conf. "Interaction of Radiation with a Solid"* (Minsk, Belarus, September 23–25, 2015), Anishchik, V.M., Ed., Minsk: Belarus State Univ., 2015, pp. 419–421.

21. Fortov, V.E., Khrapak, A.G., and Yakubov, I.T., *Fizika neideal'noi plazmy* (Physics of Non-Ideal Plasma), Moscow: Fizmatlit, 2004.

22. Bouchoule, A., *Dusty Plasmas: Physics, Chemistry and Technological Impacts in Plasma Processing*, Chichester: Wiley, 1999.

23. Kirsanov, V.V., Suvorov, A.L., and Trushin, Yu.V., *Protsessy radiatsionnogo defektoobrazovaniya v metallakh* (Processes of Radiation-Induced Defect Formation in Metals), Moscow: Energoatomizdat, 1993.

24. Lehman, C., *Interaction of Radiation with Solids and Elementary Defect Production*, Oxford, 1977.

25. Burenkov, A.F., Komarov, F.F., Kumakhov, M.A., and Temkin, M.M., *Tables of Ion Implantation Spatial Distributions*, New York: Gordon and Breach, 1986.

26. *Phase Transformations During Irradiation*, Nolfi, Jr., F.V., Ed., London–New York: Appl. Sci., 1983.

27. Kurz, W. and Fisher, D.J., *Fundamental of Solidification*, Stafa–Zurich: Trans. Tech., 1998.

28. Frenkel, Ya.I., *Kinetic Theory of Liquids*, New York: Dover, 1955.

29. Ziman, J.M., *Electrons and Phonons*, Clarendon: Oxford Univ. Press, 1960.

30. Mukhin, K.N., *Eksperimental'naya yadernaya fizika* (Experimental Nuclear Physics), Moscow: Energoatomizdat, 1993.

31. Kulikov, I.S., *Termodinamika karbidov i nitridov* (Thermodynamics of Carbides and Nitrides), Chelyabinsk: Metallurgiya, 1988.

32. *Gase und Kohlenstoff in Metallen*, Fromm, E. and Gebhardt, E., Hrsg., Berlin: Springer, 1976.

33. Nicolis, G. and Prigogine, I., *Self-Organization in Nonequilibrium Systems: From Dissipative Structures to Order Through Fluctuations*, New York–London: Wiley, 1977.

34. Flemings, M., *Solidification Processing*, New York: McGraw-Hill, 1974.

35. Linchevskii, B.V., *Vakuumnaya metallurgiya stali i splavov* (Vacuum Metallurgy of Steel and Alloys), Moscow: Metallurgiya, 1970.

36. Knuppel, H., *Desoxydation und Vakuumbehandlung von Stahlschmelzen*, Düsseldorf: Stahleisen, 1970.

37. Gabovich, M.D., Pleshivtsev, N.V., and Semashko, N.N., *Ion and Atomic Beams for Controlled Fusion and Technology*, New York: Springer, 1989.

38. Mesyats, G.A., *Vzryvnaya elektronnaya emissiya* (Explosive Electron Emission), Moscow: Fizmatlit, 2011.

Translated by Sh. Galyaltdinov